Viscous Sublayering for Shallow Water Flows

Jörn Thies Frings

Bericht Nr. 368 **Juni 2013**

Key words: multilayer flows, shallow water,
approximate Riemann solvers, finite volume method,
viscosity, friction

AMS Subject Classifications: 65M08, 76D05, 76F10, 86A05

Institut für Geometrie und Praktische Mathematik
RWTH Aachen

Templergraben 55, D–52056 Aachen (Germany)

Email address: frings@igpm.rwth-aachen.de (Jörn Thies Frings)

Preprint submitted to Applied Numerical Mathematics, June 27, 2013

Viscous Sublayering for Shallow Water Flows

Jörn Thies Frings

IGPM, RWTH Aachen, Templergraben 55, 52055 Aachen, Germany

Abstract

Analyzing the non-dimensional, incompressible Navier-Stokes equations assuming mostly laminar Shallow Water flow we deduct a set of equations modeling the evolution of mass and discharge including the effects of advection, pressure and viscosity. A numerical scheme for this system of equations is defined, where advection and pressure are dealt with by a Finite Volume approach based on the Roe solver and the viscous effects give rise to discrete velocity profiles influencing the propagation of discharge. Compared to similar works of Gerbeau/Perthame, 2001, [15] and Audusse, 2005, [2] on viscous shallow water flows we seek low numerical cost without prescribing the general shape of the velocity profiles.

Keywords: multilayer flows, shallow water, approximate Riemann solvers, finite volume method, viscosity, friction

1. Introduction

In this paper we are interested in studying Shallow Water models which allow for friction and viscous effects as well as in developing a corresponding extension for a Shallow Water Finite Volume scheme based on the Roe solver. Starting from the Navier-Stokes equations for incompressible flows, we follow the lines of Gerbeau and Perthame [15] and Audusse [2] in developing models for non-dimensional, depth-averaged models for shallow flows including a viscous term in the discharge equation and respecting a friction condition at the bottom. Along with slowing down the flow, this bottom friction gives rise to non-trivial vertical profiles for the horizontal velocities. Comparing to a simple friction condition proportional to the mean velocity of the flow, the two models of [15] and [2] allow for a better modeling of the effects of friction and viscosity. The resulting solvers compute numerical solutions closer to the solutions gained by a solver for the full Navier-Stokes equations while keeping most of the numerical efficiency of the Shallow Water solvers, as is studied in the papers mentioned.

Inspired by recent research [8] done on density-layered Shallow Water flows, [10, 12, 11, 9, 7, 1], we try to develop extended models and corresponding numerical schemes for density-layered flows that include the main effects of

Email address: frings@igpm.rwth-aachen.de (Jörn Thies Frings)

inter-layer friction and viscosity (cf. e.g. [13] for multi-layer methods including inter-layer friction). So, the model and solver described in the following should be understood as one building block for a Roe-type Finite Volume solver for the density-layered Shallow Water equation, cf. [14]. Nevertheless, in the present paper we will only consider situations with one constant density in all of the domain occupied by the flow.

Compared to [15], we tried to avoid assuming a quadratic profile for the horizontal velocities, because in the density-layered case, as well as in any other case with a nontrivial stress at the surface, we will have to deal with different kinds of friction conditions at the bottom, the surface and eventually the interface(s). Compared with [2] and the further refinements and enhancements of this approach, cf. [3, 4] and the reference therein, we sought to reduce the computational effort, as we want to apply the presented techniques for the single layer flow with constant density to each layer of a density layered flow with friction and viscosity. Also we were staying close to the Roe-type solver approach of, e.g., [9] and fitted our approach to this specific type of solver.

The system of equations which we wish to solve is of the form

$$\partial_t U + \partial_x F(U) = S(U, \partial_x b) + \mathcal{V}, \tag{1.1}$$

where U denotes a vector of water height and depth-averaged horizontal discharge, S denotes a bottom topography source term and $\mathcal{V}$ denotes a viscous term. Our approach to aprroximate a solution to this system is to introduce a vertical discretization of horizontal velocities and to apply a splitting to the time step. Thus, we consider cell-wise averaged data U_i^n and velocity vectors v_i^n (defined in Section 4). Neglecting the viscous term $\mathcal{V}$ at first, we derive auxilliary values U_i^{n*} and v_i^{n*} using an extension of a standard Finite Volume scheme for Shallow Water equations with bottom topography source term. Then, in the second step of the splitting, a correction of the velocity vectors and the depth-averaged discharges is calculated. This correction is based on an implicit discretization of the viscous term.

Formally, the solver takes the form:

$$\left.\begin{aligned} \left(U_i^{n*}, v_i^{n*}\right)^T &= \mathcal{SW}_i \left(U^n, v_i^n\right), \\ \left(U_i^{n+1}, v_i^{n+1}\right)^T &= \mathcal{V}_i^n \left(U^{n*}, v_i^{n*}\right), \end{aligned}\right\} \tag{1.2}$$

with

$$\mathcal{SW}_i : \left\{ \begin{array}{rl} U_i^n \mapsto U_i^{n*} & \text{by (3.13),} \\ (U_i^n, v_i^n) \mapsto v_i^{n*} & \text{by (4.28),} \end{array} \right\} \text{for } i \in \mathbf{Z} \tag{1.3}$$

and

$$\mathcal{V}_i : \left\{ \begin{array}{rl} (U_i^{n*}, v_i^{n*}) \mapsto v_i^{n+1} & \text{by (4.39),} \\ \left(U_i^{n*}, v_i^{n+1}\right) \mapsto U_i^{n+1} & \text{by (4.5)-(4.6),} \end{array} \right\} \text{for } i \in \mathbf{Z}. \tag{1.4}$$

Splitting and layering techniques both are widely used in the shallow water and ocean modelling community, cf. e.g. [20]. Thus we base our approach on tested simulation methods.

In Section 6, among others, we show a comparison of numerical results for a test case also used in [15] and [2]. It shows the effect of bottom friction and the arising velocity profiles due to viscosity. Our scheme compares well against the other two solvers, the improved flexibility and the reduction of numerical effort do not seem to come at the cost of the quality of the solution.

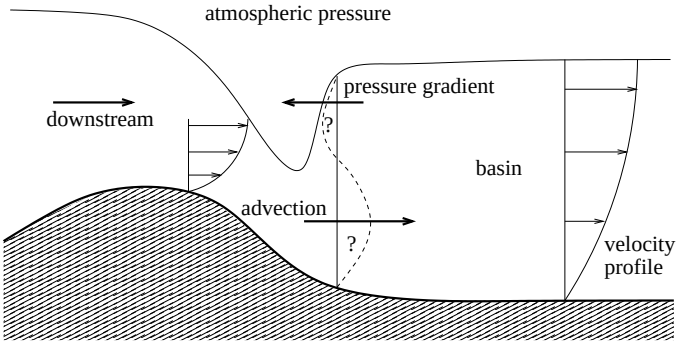

Figure 1.1: generic transcritical flow with shock, local influence of advection and pressure gradient

Another interesting question beside the profiles due to surface and bottom friction was the local differences in acceleration due to the different driving force and thus the local balance of advection, the pressure gradient and the viscosity. A typical situation of interest would be a transcritical flow over a hump, with fast flowing water accelerating at the downstream side of a hump, meeting a slow flowing basin at the base of the hump, hence forming a shock. In a steady or near steady situation, we will also find a jump in heights between these regions of different velocities, yielding equal or almost equal discharges despite the jump in velocities. Here the classical assumption of constant velocities as well as the assumption of quadratic profiles seem to be unphysical as we expect advection driving the flow downstream at the bottom of the flow, whereas at the surface of the basin we expect the pressure gradient to drive the flow upstream as pressure jumps from water pressure to atmospheric pressure, cf. Figure 1.1. In between, probably balancing both influences, we expect deflected parts of the supercritical flow and the viscosity to dissipate the downstream velocity leading to the simple constant or quadratic velocity profiles somewhere behind the shock. Closely behind the shock, we expect more sophisticated profiles including recirculation of the flow. In our approach, we tried to account for the different water heights and velocities, and hence for the different contact regions and local velocities, where local means local in depth-direction.

2. Model equations

2.1. Navier-Stokes equations

The spatial domain on which we consider the Shallow Water flow is described by x-coordinates giving the horizontal position and z-coordinates giving the

vertical one. The flow occupies a region described by a lower boundary given by the bottom-topography $z = b = b(x)$ and an upper boundary, the surface, given by $z = \eta = \eta(x,t)$. The state of the flow is described by the velocities $u = u(x,z,t)$ in x direction and $w = w(x,z,t)$ in z direction and evolves in time according to the incompressible Navier-Stokes equations ([15, 2]):

$$\partial_x u + \partial_z w = 0, \tag{2.1}$$

$$\partial_t u + \partial_x u^2 + \partial_z(wu) + \partial_x p = \partial_x \sigma_{xx} + \partial_z \sigma_{xz}, \tag{2.2}$$

$$\partial_t w + \partial_x(wu) + \partial_z w^2 + \partial_z p = -g + \partial_z \sigma_{zz} + \partial_x \sigma_{zx} \tag{2.3}$$

with

$$t > 0, \quad x \in \mathbb{R}, \quad b(x,t) \leq z \leq \eta(t,x), \tag{2.4}$$

where g is the gravitational constant and the viscosity tensor σ is given by:

$$\sigma = \begin{pmatrix} \sigma_{xx} & \sigma_{xz} \\ \sigma_{zx} & \sigma_{zz} \end{pmatrix}, \tag{2.5}$$

with

$$\sigma_{xx} = 2\mu\partial_x u, \qquad \sigma_{xz} = \mu(\partial_z u + \partial_x w), \tag{2.6}$$

$$\sigma_{zz} = 2\mu\partial_z w, \qquad \sigma_{zx} = \mu(\partial_z u + \partial_x w), \tag{2.7}$$

where μ is the viscosity constant.

The total stress tensor is then given by (cf. [4]):

$$\sigma_T = -p\, Id + \sigma. \tag{2.8}$$

We consider the system (2.1)-(2.3) together with a no-stress and a kinematic condition at the surface in addition to a no-penetration and a Navier friction condition at the bottom.

The no-stress condition reads as:

$$\sigma_T \cdot n_S = 0 \quad \text{for } z = \eta(t,x), \tag{2.9}$$

where n_S is the outward normal vector at the surface and the kinematic condition reads as

$$w - u\partial_x b - \partial_t \eta = 0 \qquad \text{for } z = b(x). \tag{2.10}$$

The Navier condition at the bottom is given by (cf. [4]):

$$t_b^T \cdot \sigma_T n_b = \kappa t_b \cdot \begin{pmatrix} u \\ w \end{pmatrix} \qquad \text{for } z = b(x), \tag{2.11}$$

where κ is a friction coefficient and t_b, n_b are unit vectors parallel and normal to the bottom:

$$t_b := \frac{1}{(1 + (\partial_x b)^2)^{\frac{1}{2}}} \begin{pmatrix} 1 \\ \partial_x b \end{pmatrix}, \tag{2.12}$$

$$n_b := \frac{1}{(1 + (\partial_x b)^2)^{\frac{1}{2}}} \begin{pmatrix} -\partial_x b \\ 1 \end{pmatrix}, \tag{2.13}$$

thus the stress along the bottom is estimated by κ times the velocity parallel to the bottom. The no-penetration condition at the bottom is given by:

$$w - u\partial_x b = 0 \qquad \text{for } z = b(x), \tag{2.14}$$

therefore the velocity perpendicular to b vanishes at the bottom.

2.2. Non-dimensional Navier-Stokes equations

Introducing characteristic reference values we can derive non-dimensional equations. The characteristic height z_{ref} and the characteristic length x_{ref} are connected by the constant ratio $\varepsilon = z_{ref}/x_{ref}$. The Shallow Water assumption now states that ε is small in some sense which allows us to drop certain terms in the equations due to scaling arguments. So we also introduce characteristic values for the horizontal and vertical velocities, u_{ref} and w_{ref}, and the time, t_{ref}, connected by the equation $u_{ref} = x_{ref}/t_{ref}$, leading to the non-dimensional, incompressible Navier-Stokes equations, which are given as (rescaled variables are denoted by the same letter as the original ones, cf. [15]):

$$\partial_x u + \partial_z w = 0, \tag{2.15}$$

$$\partial_t u + \partial_x u^2 + \partial_z(wu) + \partial_x p = 2\nu\partial_{xx}u + \frac{\nu}{\varepsilon^2}\partial_{zz}u + \nu\partial_{xz}w, \tag{2.16}$$

$$\varepsilon^2\left[\partial_t w + \partial_x(wu) + \partial_z w^2\right] + \partial_z p = -G + \varepsilon^2\nu\partial_{xx}w + 2\nu\partial_{zz}w + \nu\partial_{xz}u \tag{2.17}$$

where

$$\text{(i) } \varepsilon = \frac{z_{ref}}{x_{ref}}, \qquad \text{(ii) } \nu = \frac{\mu}{u_{ref}x_{ref}}, \qquad \text{(iii) } \frac{1}{G} := F^2 := \frac{(u_{ref})^2}{g z_{ref}}. \tag{2.18}$$

The kinematic condition at the free surface $\eta = \eta(x,t)$ transforms to:

$$w = \partial_t\eta + u\partial_x\eta, \qquad \text{for } z = \eta(x,t) \tag{2.19}$$

and the no-stress conditions $\sigma_T \cdot n_S = 0$ become

$$\frac{1}{F^2}p\partial_x\eta + \nu\left[\frac{1}{\varepsilon^2}\partial_z u - 2\partial_x u\partial_x\eta + \partial_x w\right] = 0, \qquad \text{for } z = \eta(x,t), \tag{2.20}$$

$$\frac{1}{F^2}p + \nu\left[-2\partial_z w + \partial_z u\partial_x\eta + \varepsilon^2\partial_x w\partial_x\eta\right] = 0 \qquad \text{for } z = \eta(x,t). \tag{2.21}$$

At the bottom we have the kinematic condition

$$w - u\partial_x b = 0, \qquad \text{for } z = b(x,t). \tag{2.22}$$

The Navier friction condition reads, using the $0 = \frac{d}{dx}(w - u\partial_x b)$ for $z = b(x)$:

$$\frac{\nu}{\varepsilon}\left(\partial_z u - \varepsilon^2\partial_x w\right) = \gamma\left(1 - 2\frac{\varepsilon}{x_{ref}}\partial_{xx}b\right)u \qquad \text{for } z = b(x,t), \tag{2.23}$$

where $\gamma := \kappa/u_{ref}$ is the non-dimensional friction coefficient.

2.3. Classical hydrostatic model

As also described in [15] and [2], we continue our simplification with the assumption that the viscosity and friction coefficients depend on the Shallow Water coefficient ε:

$$\nu = \varepsilon\nu_0, \qquad \gamma = \varepsilon\gamma_0. \tag{2.24}$$

With these assumptions and the Shallow Water assumption stated above we can simplify the equation by neglecting terms with the factors ε, ε^2, ε^3:

$$\partial_x u + \partial_z w = 0, \tag{2.25}$$

$$\partial_t u + \partial_x u^2 + \partial_z(wu) + \partial_x p = \frac{\nu_0}{\varepsilon}\partial_{zz} u, \tag{2.26}$$

$$\partial_z p = -G. \tag{2.27}$$

Also the boundary conditions can be simplified with this approach. The kinematic condition at the free surface $\eta = \eta(x,t)$ simplifies to:

$$w = \partial_t \eta + u\partial_x \eta, \qquad \text{for } z = \eta(x,t) \tag{2.28}$$

and the no-stress conditions $\sigma_T \cdot n_S = 0$ become

$$\frac{\nu_0}{\varepsilon}\partial_z u = 0 \qquad \text{for } z = \eta(x,t), \tag{2.29}$$

$$p = 0 \qquad \text{for } z = \eta(x,t). \tag{2.30}$$

At the bottom we have the no-penetration condition

$$w = u\partial_x b, \qquad \text{for } z = b(x,t). \tag{2.31}$$

The Navier friction condition reads

$$\gamma_0 u = \frac{\nu_0}{\varepsilon}\partial_z u, \qquad \text{for } z = b(x,t). \tag{2.32}$$

In all of the above we kept the terms with ν_0/ε, as we are interested in the influence of the viscosity on the horizontal velocity.

From the equations (2.27) and (2.30) we can deduct the hydrostatic pressure equation:

$$p(x,z,t) = G(\eta(x,t) - z). \tag{2.33}$$

This equation will later be used to simplify the equation 2.26 further.

2.4. Depth-integrated equations

By integrating in the z-direction and exploiting the incompressibility of the flow we obtain the depth-integrated equations. First, the continuity equation

(2.25) together with the kinematic condition (2.28) and the no-penetration condition gives:

$$\begin{aligned}
0 &= \int_{b(x)}^{\eta(x,t)} \partial_x u \, \mathrm{d}z + \int_{b(x)}^{\eta(x,t)} \partial_z w \, \mathrm{d}z \\
&= \partial_x \int_{b(x)}^{\eta(x,t)} u \, \mathrm{d}z + u(x, b(x), t)\partial_x b - u(x, \eta(x,t), t)\partial_x \eta \\
&\quad + w(x, \eta(x,t), t) - w(x, b(x), t) \\
&= \partial_x \int_{b(x)}^{\eta(x,t)} u \, \mathrm{d}z + \partial_t \eta \\
&= \partial_x h\bar{u} + \partial_t h, \qquad (2.34)
\end{aligned}$$

where $h(x,t) = \eta(x,t) - b(x)$ is the thickness of the flow and

$$\bar{u} = \frac{1}{h(x,t)} \int_{b(x)}^{\eta(x,t)} u \, \mathrm{d}z \qquad (2.35)$$

is the depth-averaged horizontal velocity. Integrating the discharge equation (2.26) using the hydrostatic pressure (2.33) yields:

$$\begin{aligned}
\int_{b(x)}^{\eta(x,t)} \frac{\nu_0}{\varepsilon} \partial_{zz} u \, \mathrm{d}z &= \int_{b(x)}^{\eta(x,t)} \partial_t u + \partial_x u^2 + \partial_z (wu) + \partial_x p \, \mathrm{d}z \\
&= \partial_t h\bar{u} - u(x,\eta,t)\left(\partial_t \eta - w(x,\eta,t) + u(x,\eta,t)\partial_x \eta\right) \\
&\quad + u(x,b,t)\left(\partial_t b + u(x,b,t)\partial_x b - w(x,b,t)\right) \\
&\quad + \partial_x h\bar{u}^2 + \frac{G}{2}\partial_x h^2 + Gh\partial_x b \\
&= \partial_t h\bar{u} + \partial_x \left[h\bar{u}^2 + \frac{G}{2}h^2\right] + Gh\partial_x b, \qquad (2.36)
\end{aligned}$$

where we used

$$\int_{b(x)}^{\eta(x,t)} u^2 \, \mathrm{d}z = \bar{u}^2 \qquad (2.37)$$

to first order, cf. [15]. Thus, we derived a system of equations together with the no-stress and Navier friction conditions (2.29), (2.32):

$$\partial_t h + \partial_x h\bar{u} = 0, \qquad (2.38)$$

$$\partial_t h\bar{u} + \partial_x \left[h\bar{u}^2 + \frac{G}{2}h^2\right] = -Gh\partial_x b + \frac{\nu_0}{\varepsilon}\left[\partial_z u(x.\eta(x,t),t) - \partial_z u(x, b(x), t)\right]. \qquad (2.39)$$

This can be written in the form:

$$\partial_t U + \partial_x F(U) = S(U, \partial_x b) + \mathcal{V}, \qquad (2.40)$$

where $U = (h, h\bar{u})^T$, and

$$F(U) = \begin{pmatrix} h\bar{u} \\ h\bar{u}^2 + \frac{G}{2}h^2 \end{pmatrix}, \tag{2.41}$$

$$S(U, \partial_x b) = \begin{pmatrix} 0 \\ -Gh\partial_x b \end{pmatrix}, \tag{2.42}$$

$$\mathcal{V} = \frac{\nu_0}{\varepsilon} \left[\partial_z u(x, \eta(x,t), t) - \partial_z u(x, b(x), t) \right]. \tag{2.43}$$

As a special case for vanishing viscosity and friction coefficients, from this system we can derive the classical Saint-Venant system for Shallow Water flows:

$$\partial_t h + \partial_x h\bar{u} = 0, \tag{2.44}$$

$$\partial_t h\bar{u} + \partial_x \left[h\bar{u}^2 + \frac{G}{2}h^2 \right] = -Gh\partial_x b. \tag{2.45}$$

This model, a balance law, i.e., a conservation law with source term, is thoroughly analyzed in various publications and there exists a variety of solvers (see e.g. [6, 18] and the references therein).

For numerically solving the depth-averaged viscous model (2.38)-(2.39) we thus try to build upon a numerical scheme for solving the underlying Saint-Venant system (2.44)-(2.45) and add an implicit treatment of the viscous term $\mathcal{V}$, partly following [2]. In the following section we will describe the numerical scheme we are using to solve the Saint-Venant system and in Section 4 we will describe our treatment of the viscous term. The main idea is to introduce discrete velocity profiles that are updated according to the underlying balance law (2.44)-(2.45) and reflect the effect of friction and viscosity on the horizontal velocities.

3. Finite Volume scheme

We discretize (2.44)-(2.45) using a Finite Volume method based on Roe's Riemann solver, cf. [19] or [17, 6]. We use a uniform grid with cells $[x_{i-1/2}, x_{i+1/2}]$ and grid-size $\Delta x = x_{i+1/2} - x_{i-1/2}$. The midpoints of the cells are denoted by $x_i := 1/2 \left(x_{i-1/2} + x_{i+1/2} \right)$. Likewise, we discretize the time by $t^{n+1} = t^n + \Delta t^n$, where the time step sizes $\Delta t^n > 0$ are chosen according to a CFL-condition, see (5.6).

For exact solutions of (2.44)-(2.45) the cell average over the i^{th} cell

$$U_i(t) := \frac{1}{\Delta x} \int_{x_{i-\frac{1}{2}}}^{x_{i+\frac{1}{2}}} U(x,t)\, dx, \tag{3.1}$$

satisfies

$$\begin{aligned} \frac{d}{dt} U_i(t) = &-\frac{1}{\Delta x} \left(F(U(x_{i+\frac{1}{2}}, t)) - F(U(x_{i-\frac{1}{2}}, t)) \right) \\ &+ \frac{1}{\Delta x} \int_{x_{i-\frac{1}{2}}}^{x_{i+\frac{1}{2}}} S(U(x,t), \partial_x b) dx. \end{aligned} \tag{3.2}$$

We approximate these cell averages at time t^n by the discrete values

$$\begin{pmatrix} h_i^n \\ h_i^n u_i^n \end{pmatrix} =: U_i^n \approx U_i(t^n). \tag{3.3}$$

Note that while we do no longer use a bar over u_i^n, it should still be understood as an approximation of the *averaged* horizontal velocity.

Following [5], we will derive a splitting of the right hand side of (3.2) and define an update of the form

$$\frac{U_i^{n*} - U_i^n}{\Delta t} := -\frac{1}{\Delta x}\left(\mathcal{A}^-_{i+\frac{1}{2}} - \mathcal{A}^+_{i-\frac{1}{2}}\right), \tag{3.4}$$

and set $U_i^{n+1} := U_i^{n*}$. The notation in this form is in preparation of the following section. The numerical fluxes $\mathcal{A}^-_{i+1/2}$ and $\mathcal{A}^+_{i-1/2}$ are derived in the following (see (3.12) below for their final form). They contain the discretizations of both the numerical fluxes and the source term. Of course, they depend on the time step t^n as well as on the spatial position. For convenience of notation, we will not denote the dependency on the current time step explicitely and drop the superscript n in other terms as well when this dependency is not ambiguous.

We now review the splitting in [5]. We fix the cell interface $x_{i+1/2}$ and denote the Roe matrix with left and right states U_i and U_{i+1} by

$$\tilde{A}_{i+\frac{1}{2}} := A(\tilde{U}_{i+\frac{1}{2}}), \tag{3.5}$$

where $\tilde{U}_{i+1/2} = (\tilde{h}_{i+1/2}, \tilde{h}_{i+1/2}\tilde{u}_{i+1/2})^T$ is given by

$$\tilde{h}_{i+\frac{1}{2}} = \frac{h_i + h_{i+1}}{2}, \qquad \tilde{u}_{i+\frac{1}{2}} = \frac{u_i\sqrt{h_i} + u_{i+1}\sqrt{h_{i+1}}}{\sqrt{h_i} + \sqrt{h_{i+1}}}. \tag{3.6}$$

Note that we have Roe's conservation property, cf. [19]:

$$F(U_{i+1}) - F(U_i) = \tilde{A}_{i+\frac{1}{2}}(U_{i+1} - U_i), \tag{3.7}$$

The source term is discretized by

$$\tilde{S}_{i+\frac{1}{2}} := \begin{pmatrix} 0 \\ -G\tilde{h} \end{pmatrix} \frac{b_{i+1} - b_i}{\Delta x}\Delta x \approx \int_{x_{i-\frac{1}{2}}}^{x_{i+\frac{1}{2}}} S(U(x,t), \partial_x b)dx. \tag{3.8}$$

Now we decompose the differences $U_{i+1} - U_i$ and $F(U_{i+1}) - F(U_i) - \tilde{S}_{i+1/2}$ into eigenvectors of the Roe matrix. For this, let

$$\tilde{A}_{i+\frac{1}{2}} = R\Lambda R^{-1}, \tag{3.9}$$

where the diagonal matrix Λ contains the eigenvalues $\lambda^1, \ldots, \lambda^m$ of $\tilde{A}_{i+1/2}$ and $R = (r^1, \ldots, r^m)$ is the matrix of right eigenvectors. Then there are scalars

α^p, β^p such that

$$U_{i+1} - U_i = \sum_p \alpha^p r^p_{i+\frac{1}{2}} =: \sum_p \mathcal{W}^p_{i+\frac{1}{2}}, \tag{3.10}$$

$$F(U_{i+1}) - F(U_i) - \Delta x \tilde{S}_{i+\frac{1}{2}} = \sum_p \beta^p r^p_{i+\frac{1}{2}} =: \sum_p \mathcal{Z}^p_{i+\frac{1}{2}}. \tag{3.11}$$

These decompositions exist and are unique, since we postulate hyperbolicity of the Roe matrices, i.e., the Roe matrices have to have a full set of real eigenvalues, cf. [19].

Then, the numerical fluxes are obtained as:

$$\mathcal{A}^-_{i+\frac{1}{2}} = F(U_i) + \sum_{p:\lambda_p<0} \mathcal{Z}^p_{i+\frac{1}{2}}, \qquad \mathcal{A}^+_{i+\frac{1}{2}} = F(U_{i+1}) - \sum_{p:\lambda_p>0} \mathcal{Z}^p_{i+\frac{1}{2}} \tag{3.12}$$

Together with (3.4) this finishes the definition of the Finite Volume scheme. Below, we will also use the equivalent update formula

$$U_i^{n*} = U_i^n - \frac{\Delta t^n}{\Delta x} \left(\sum_{p:\lambda_p<0} \mathcal{Z}^p_{i+\frac{1}{2}} + \sum_{p:\lambda_p>0} \mathcal{Z}^p_{i-\frac{1}{2}} \right). \tag{3.13}$$

4. Velocity profiles

In this section we describe our numerical treatment of the viscous term $\mathcal{V}$ in (2.40). The treatment will be based on discrete vertical profiles of the horizontal velocity. Like in the derivation of a multilayer Shallow Water solver in [2], we assume that the flow is mainly laminar. Hence, we subdivide the flow in the vertical direction to gain information on the dominating velocity u depending on the z position, when bottom friction and viscous forces are considered.

We subdivide the flow vertically in N layers, separated by the curves η_j:

$$\eta_j(x,t) := (1 - \frac{j}{N})h(x,t) + b(x), \quad j = 0, \ldots, N, \tag{4.1}$$

so that η_0 gives the height of the surface over the reference level, η_N is equal to the bottom elevation, and $\eta_{j-1} - \eta_j = h(x,t)/N$, $j = 1, \ldots, N$, $(x,t) \in \mathbb{R} \times \mathbb{R}^+$. We set $z_j(x,t) = \eta_j - h(x,t)/N$, $j = 1, \ldots, N$, i.e., z_j is the middle line of the j^{th} layer.

We define the horizontal velocities $v_j(x,t)$ which can be interpreted as the velocities at z_j or even the mean velocities of the flow within the layers, i.e., v_j is the mean velocity of the flow between η_{j-1} and η_j.

We can also define discrete versions of these functions written in terms of the discrete heights and discharges used in the Finite Volume approach mentioned in the previous section. For each cell i we have, at time $t = t^n$:

$$\eta^n_{i,j} := (1 - \frac{j}{N})h^n_i + b_i, \quad j = 0, \ldots, N, \tag{4.2}$$

describing a subdivision of the discretized flow in this cell into N layers. The values $z_{i,j}^n := \eta_{i,j}^n - h_i^n/N$, $j = 1, \dots, N$ give the midpoints of the layers in vertical direction.

The velocity vector $v_i^n := \left(v_{i,j}^n\right)_{j=1..N} := \left(v_j(x_i, t^n)\right)_{j=1..N}$ is meant to describe the discrete vertical velocity profile of the i^{th} cell. Introducing the notation $q_i^n := h_i^n u_i^n$ for the horizontal discharge, we postulate the following consistency condition between the velocity vectors and the data $(h_i^n, h_i^n u_i^n)^T$:

$$\sum_{j=1}^{N} \frac{h_i^n}{N} v_{i,j}^n = h_i^n u_i^n = q_i^n \qquad \text{for } i \in \mathbb{Z}. \tag{4.3}$$

Now, we want to use these discrete velocity profiles to approximate solutions of (2.38)-(2.39). For this, we employ a Finite Volume method based on Roe's solver like in (3.13) together with a discretization of the viscous term $\mathcal{V}$ based on the discrete velocity profiles.

The strategy will be the following: starting with the cell-wise averaged data U_i^n defined by (3.3) and consistent velocity vectors v_i^n we subdivide the time step $t^n \to t^{n+1}$ in the following steps:

Step 1 Calculate the auxiliary values $U_i^{n*} := (h_i^{n*}, q_i^{n*})^T$ as solution to the discretized balance law (3.13).

Step 2 Distribute the update of Step 1 among the entries of the velocity vectors v_i^n to derive auxiliary velocity vectors v_i^{n*} in consistency with U_i^{n*}:

$$\sum_{j=1}^{N} \frac{h_i^{n*}}{N} v_{i,j}^{n*} = q_i^{n*} \qquad \text{for } i \in \mathbb{Z}. \tag{4.4}$$

Step 3 Use the v_i^{n*} in an implicit discretization of the viscous terms to derive the discrete profile v_i^{n+1}.

Step 4 Define $U_i^{n+1} := (h_i^{n+1}, q_i^{n+1})^T$ by:

$$h_i^{n+1} := h_i^{n*} \qquad \text{for } i \in \mathbb{Z}, \tag{4.5}$$

$$q_i^{n+1} := \sum_{j=1}^{N} \frac{h_i^{n+1}}{N} v_{i,j}^{n+1} \qquad \text{for } i \in \mathbb{Z}, \tag{4.6}$$

such that the consistency of v_i^{n+1} and U_i^{n+1} according to 4.3 is enforced by definition.

In Step 2 the numerical fluxes in the total discharge component are weighted in a way that the velocity vectors v_i^{n*} will automatically be consistent with q_i^{n*}, as described below in 4.1. To gain the v_i^{n+1}, only discrete viscous terms and the auxiliary profile v_i^{n*} are considered in Step 3, cf. Section 4.2.

Thus, we have a mutual influence: first, the depth averaged data gives an update for the velocity profiles. Then, after considering the effects of viscosity

on the velocity profiles, the updated profiles are used in the definition of the depth averaged data at the new time step.

Finally, defining the sequences $U^{\cdot} := \{U_i^{\cdot}\}_{i\in\mathbf{Z}}$ and $v^{\cdot} := \{v_i^{\cdot}\}_{i\in\mathbf{Z}}$, for given data U^n, v^n we will derive a solver of the form

$$\left.\begin{aligned}(U_i^{n*}, v_i^{n*})^T &= \mathcal{SW}_i\left(U^n, v^n\right),\\ \left(U_i^{n+1}, v_i^{n+1}\right)^T &= \mathcal{V}_i^n\left(U^{n*}, v^{n*}\right),\end{aligned}\right\} \tag{4.7}$$

where the operators $\mathcal{SW}_i$ are based on explicit Finite Volume update formulas as given in (3.13) and weighted Finite Volume update formulas as defined in Section 4.1. The operators $\mathcal{V}_i^n$ are defined using discretizations of the viscous term $\mathcal{V}$ in cell i at time t^n and the definition (4.5)-(4.6), as detailed in Section 5.

4.1. Update formula for the discrete velocity profiles

In addition to the Finite Volume method of Step 1 we need to define a way to update the discrete velocity vector in accordance with the balance law (2.40). In Step 1 we solve a discretized balance law like in (3.13):

$$\frac{U_i^{n*} - U_i^n}{\Delta t^n} = -\frac{1}{\Delta x}\left(\mathcal{A}^-_{i+\frac{1}{2}} - \mathcal{A}^+_{i-\frac{1}{2}}\right), \tag{4.8}$$

where the result denoted by U_i^{n*} is an auxiliary value. In Step 2, the result of the advection step for the total heights and discharges needs to be distributed to the N layers to gain an update formula for the discrete velocity profile. Starting with the assumption

$$\sum_{j=1}^{N} \frac{h_i^n}{N} v_{i,j}^n = h_i^n u_i^n = q_i^n, \tag{4.9}$$

we want to find a formula defining the values $v_{i,j}^{n*}$ such that

$$\sum_{j=1}^{N} \frac{h_i^{n*}}{N} v_{i,j}^{n*} = q_i^{n*} \tag{4.10}$$

holds, where q_i^{n*} is the result for the discharge update of the above solver (4.8) for the balance law.

As described above we want to distribute the update contribution from the numerical fluxes at the cell boundaries among the layers, i.e., among the discrete velocity profiles. We will examine these numerical fluxes for the depth-averaged quantities U_i^n now. The left and right numerical fluxes $\mathcal{A}^-_{i+1/2}$, $\mathcal{A}^+_{i+1/2}$ for this update are defined by the Roe solver again, thus we compute Roe intermediates $\tilde{U}_{i+1/2}$ to linearize the flux function F, yielding

$$\tilde{A}_{i+\frac{1}{2}}(U_i - U_{i+1}) = \tilde{A}_{i+\frac{1}{2}}(\sum_p \mathcal{W}^p_{i+\frac{1}{2}}) = F(U_i) - F(U_{i+1}) = \sum_p \mathcal{Z}^p_{i+\frac{1}{2}} \tag{4.11}$$

as described in Section 3. Note that we neglected the source term discretization to simplify notation, later in this section we will consider the bottom topography again.

The terms in the flux function and the corresponding terms in the linearization are associated to transport and acceleration due to a pressure gradient, i.e., to forces acting on the surface respectively the body of any given volume. In the discharge equation we have for the cell on the right of the interface, after linearization and discretization of the x and t coordinates,

$$\frac{h_i^{n*}u_i^{n*} - h_i^n u_i^n}{\Delta t^n} = -\frac{1}{\Delta x}\left(\sum_{p:\lambda_p<0} \mathcal{Z}^p_{i+\frac{1}{2}} + \sum_{p:\lambda_p>0} \mathcal{Z}^p_{i-\frac{1}{2}}\right)_{hu}, \tag{4.12}$$

where the subscript hu denotes the second, the discharge component of the vectors $\mathcal{Z}^p_{i\pm1/2}$. Now, examining the $\mathcal{Z}^p_{i+1/2}$ and $\mathcal{Z}^p_{i-1/2}$ yields:

$$\begin{aligned}
&-\frac{1}{\Delta x}\left(\sum_{p:\lambda_p \lessgtr 0} \mathcal{Z}^p_{i\pm\frac{1}{2}}\right)_{hu} \\
&= -\frac{1}{\Delta x}\left(\left(-\tilde{u}^2_{i\pm\frac{1}{2}} + G\tilde{h}_{i\pm\frac{1}{2}}\right)\mathcal{W}^{\mp}_h + 2\tilde{u}_{i\pm\frac{1}{2}}\mathcal{W}^{\mp}_{hu}\right) \\
&= -\frac{1}{\Delta x}\left(\tilde{u}_{i\pm\frac{1}{2}}\left(-\tilde{u}_{i\pm+\frac{1}{2}}\mathcal{W}^{\mp}_h + 2\mathcal{W}^{\mp}_{hu}\right) + G\tilde{h}_{i\pm\frac{1}{2}}\mathcal{W}^{\mp}_h\right)
\end{aligned} \tag{4.13}$$

where $\mathcal{W}^{\mp}_h$, $\mathcal{W}^{\mp}_{hu}$ are the parts of an eigenvector decomposition of the jumps in h and hu respectively which are associated with only positive or only negative eigenvalues:

$$\left(\mathcal{W}^+_h, \mathcal{W}^+_{hu}\right)^T = \mathcal{W}^+ = \sum_{p:\lambda_p>0} \mathcal{W}^p_{i-\frac{1}{2}} \tag{4.14}$$

$$\left(\mathcal{W}^-_h, \mathcal{W}^-_{hu}\right)^T = \mathcal{W}^- = \sum_{p:\lambda_p<0} \mathcal{W}^p_{i+\frac{1}{2}}. \tag{4.15}$$

The term $G\tilde{h}_{i\pm1/2}\mathcal{W}^{\mp}_h$ gives the influence of the pressure on the time evolution, hence we will split this term N times and distribute evenly throughout the layers.

The remaining term is a transport term and should be influenced by the local speeds $v_{i,j}$, $v_{i+1,j}$ to the left and right of the interface. We will assign vectors of weights $\omega^-_{i,j}$, $\omega^+_{i,j}$ to each cell, which depend on the local speeds at the cell interfaces such that:

$$\sum_j \omega^-_{i,j} = 1 \quad \omega^-_{i,j}\tilde{u}_{i-\frac{1}{2}} = \frac{\tilde{v}^-_{i,j}}{N}, \qquad \sum_j \omega^+_{i,j} = 1 \quad \omega^+_{i,j}\tilde{u}_{i+\frac{1}{2}} = \frac{\tilde{v}^+_{i,j}}{N}, \tag{4.16}$$

where $\tilde{v}^{\pm}_{i,j}$ are intermediate velocities at the interfaces $x_{i-1/2}$, $x_{i+1/2}$ connected to the j^{th} layer of the cell i, yet to be defined. With the condition above, these

N intermediate velocities also fulfill $\tilde{u}_{i\pm1/2} = 1/N \sum_j \tilde{v}^{\pm}_{i,j}$. They can be viewed as approximative Roe intermediates for the j^{th} layer.

To obtain the intermediate values $\tilde{v}^{-}_{i,j}$, i.e., the intermediate velocities for the cell i at the interface $x_{i-1/2}$, first we determine the layer indices j for which the lower boundary $\eta^n_{i,j}$ is smaller than the surface $\eta^n_{i-1,0}$ of the flow in the adjacent cell and the upper boundary $\eta^n_{i,j-1}$ is bigger than the bottom of the flow $\eta^n_{i-1,N}$ in the adjacent cell:

$$\mathcal{J}_i^- := \{j : \eta_{i,j-1} > \eta_{i-1,N} \wedge \eta_{i,j} < \eta_{i-1,0}\}. \tag{4.17}$$

Therefore, the layers with index in $\mathcal{J}_i^-$ intersect in z direction with the domain occupied by the flow in the adjacent cell and we have a direct physical connection between these layers and the flow on the other side of the interface. For these layers we carry out a nearest neighbor interpolation for the velocity profiles. The layer velocities $v_{i-1,j}$, $v_{i,j}$ are assigned to the layer midpoints $z_{i-1,j}$, $z_{i,j}$ and we interpolate the velocities on the left side of the interface at the layer midpoints of the right cell.

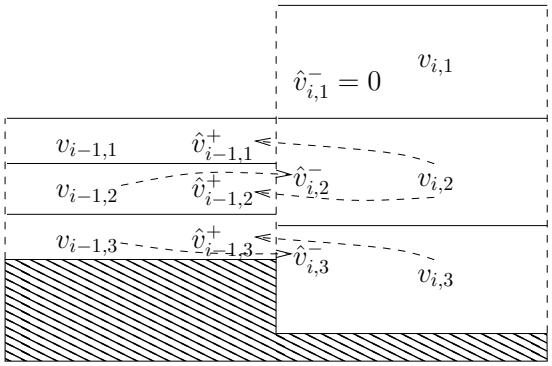

Figure 4.2: interpolation of local velocities at the cell interface, arrows indicate which value from across the interface goes in the calculation of which local speed

Hence, calculating the intermediate values for cell i with layer midpoints $z_{i,j}$ and velocities $v_{i,j}$, we determine for each layer j whether $\eta_{i,j-1} > \eta_{i-1,N}$ and $\eta_{i,j} < \eta_{i-1,0}$, i.e., whether $j \in \mathcal{J}_i^-$ holds. If not, we set $\omega^-_{i,j} = 0$, as there is no direct physical connection of this layer with the flow on the other side of the interface. Else, we take the layer midpoint z_{i-1,k_j} in the left cell which is closest to $z_{i,j}$

$$k_j^- : |z_{i-1,k_j^-} - z_{i,j}| = \min_k |z_{i-1,k} - z_{i,j}| \tag{4.18}$$

and set, see Figure 4.2

$$\hat{v}^-_{i,j} := 0.5 \cdot (v_{i,j} + v_{i-1,k_j^-}). \tag{4.19}$$

These intermediate velocities are considered local auxiliary velocities similar to Roe intermediates. When all the layers have been considered, the intermediate

values $\tilde{v}^-_{i,j}$ and thus the weights $\omega^-_{i,j}$ are set to:

$$\tilde{v}^-_{i,j} := \frac{\hat{v}^-_{i,j}}{\sum_j \hat{v}^-_{i,j}} N \tilde{u}_{i-\frac{1}{2}}, \tag{4.20}$$

$$\omega^-_{i,j} := \frac{\hat{v}^-_{i,j}}{\sum_j \hat{v}^-_{i,j}}. \tag{4.21}$$

With this definition, the intermediate velocity $\tilde{u}_{i-1/2}$ is the mean value of the values $\tilde{v}^-_{i,j}$, $j = 1, \dots, N$, which in turn depend on the local velocities to the left and the right of the interface. The values at $x_{i+1/2}$ are calculated analogously: We set

$$\mathcal{J}^+_i := \{j : \eta_{i,j-1} > \eta_{i+1,N} \wedge \eta_{i,j} < \eta_{i+1,0}\}, \tag{4.22}$$

and set $\omega^+_{i,j} = 0$ for $j \notin \mathcal{J}^+_i$, otherwise we determine

$$k^+_j : |z_{i+1,k^+_j} - z_{i,j}| = \min_k |z_{i+1,k} - z_{i,j}|. \tag{4.23}$$

Then, we use these indices to define

$$\hat{v}^+_{i,j} := 0.5 \cdot (v_{i,j} + v_{i+1,k^+_j}) \tag{4.24}$$

and

$$\tilde{v}^+_{i,j} := \frac{\hat{v}^+_{i,j}}{\sum_j \hat{v}^+_{i,j}} N \tilde{u}_{i+\frac{1}{2}}, \tag{4.25}$$

$$\omega^+_{i,j} N \tilde{u}_{i+\frac{1}{2}} := \frac{\hat{v}^+_{i,j}}{\sum_j \hat{v}^+_{i,j}}. \tag{4.26}$$

With the weights we defined in this way, we can split the discharge equation above in N equations of the form:

$$\begin{aligned}
&- \frac{1}{N\Delta x} \left(\sum_{p:\lambda_p \gtrless 0} \mathcal{Z}^p_{i\pm\frac{1}{2}} \right)_{hu} \\
&\approx -\frac{1}{\Delta x} \left(\frac{\tilde{v}^\pm_{i,j}}{N} \left(-\tilde{u}_{i\pm\frac{1}{2}} \mathcal{W}^\mp_h + 2\mathcal{W}^\mp_{hu} \right) + G \frac{\tilde{h}_{i\pm\frac{1}{2}}}{N} \mathcal{W}^\mp_h \right) \\
&= -\frac{1}{\Delta x} \left(\omega^\pm_{i,j} \tilde{u}_{i\pm\frac{1}{2}} \left(-\tilde{u}_{i\pm\frac{1}{2}} \mathcal{W}^\mp_h + 2\mathcal{W}^\mp_{hu} \right) + G \frac{\tilde{h}_{i\pm\frac{1}{2}}}{N} \mathcal{W}^\mp_h \right).
\end{aligned} \tag{4.27}$$

The sum of these N equations yields (4.13) again, as the weights $\omega^\pm_{i,j}$ and $1/N$ sum up to 1. In the second line of (4.27) we put in $\tilde{v}^\pm_{i,j}$ as a local approximation of the intermediate velocities at the left and right boundaries of layer j in cell i. This is based on the approximation $u(x, z, t) = \overline{u}(x, t) + \mathcal{O}(\varepsilon)$, which can be

shown using (2.26), (2.29) and (2.32), cf. [2, 15]. This also implies $u(x_i, z_i, t^n) = v^n_{i,j} + \mathcal{O}(\varepsilon)$, as the $v^n_{i,j}$ are bound to $\overline{u}$ by the consistency condition and to each other by viscosity, as will be shown in (4.39).

Hence, based on the eigenvector decomposition of the jumps in the total height and the total discharge, we can define an update of the discharge $h^n_i/N v^n_{i,j}$ in the j^{th} layer at time t^n using (4.27):

$$\frac{h^{n*}_i}{N} v^{n*}_{i,j} - \frac{h^n_i}{N} v^n_{i,j} = -\frac{\Delta t^n}{\Delta x} \left(\omega^+_{i,j} \tilde{u}_{i+\frac{1}{2}} \left(-\tilde{u}_{i+\frac{1}{2}} \mathcal{W}^-_h + 2\mathcal{W}^-_{hu} \right) + G \frac{\tilde{h}_{i+\frac{1}{2}}}{N} \mathcal{W}^-_h \right.$$
$$\left. + \omega^-_{i,j} \tilde{u}_{i-\frac{1}{2}} \left(-\tilde{u}_{i-\frac{1}{2}} \mathcal{W}^+_h + 2\mathcal{W}^+_{hu} \right) + G \frac{\tilde{h}_{i-\frac{1}{2}}}{N} \mathcal{W}^+_h \right). \tag{4.28}$$

After these update formulas are applied, we achieve the discharges $h^{n*}_{i+1}/N v^{n*}_{i,j}$ and thus a new velocity vector v^{n*}_i. Note that by the definition of the weights, the N discharge equations (4.28) simply add up to the equation for the total discharge (4.12).

To be able to write down the update formula for the N layers and to simplify the inclusion of the source terms we will split the whole update N times and write it down in terms of f-waves:

$$\sum_{p:\lambda_p \lessgtr 0} \mathcal{Z}^p_{i\pm\frac{1}{2}} = \tilde{\mathcal{A}}_{i\pm\frac{1}{2}} \mathcal{W}^\mp = \begin{pmatrix} \mathcal{W}^\mp_{hu} \\ \tilde{u}_{i\pm\frac{1}{2}} \left(-\tilde{u}_{i\pm\frac{1}{2}} \mathcal{W}^\mp_h + 2\mathcal{W}^\mp_{hu} \right) + G\tilde{h}_{i\pm\frac{1}{2}} \mathcal{W}^\mp_h \end{pmatrix} \tag{4.29}$$

$$\Leftrightarrow \sum_{p:\lambda_p \lessgtr 0} \mathcal{Z}^p_{i\pm\frac{1}{2}} - \begin{pmatrix} \mathcal{W}^\mp_{hu} \\ G\tilde{h}_{i\pm\frac{1}{2}} \mathcal{W}^\mp_h \end{pmatrix} = \begin{pmatrix} 0 \\ \tilde{u}_{i\pm\frac{1}{2}} \left(-\tilde{u}_{i\pm\frac{1}{2}} \mathcal{W}^\mp_h + 2\mathcal{W}^\mp_{hu} \right) \end{pmatrix}. \tag{4.30}$$

Now, setting

$$\mathcal{T}^p_{i+\frac{1}{2}} = \begin{pmatrix} 0 & 1 \\ G\tilde{h}_{i+\frac{1}{2}} & 0 \end{pmatrix} \mathcal{W}^p_{i+\frac{1}{2}}, \tag{4.31}$$

we can formally write down the update formula for the j^{th} layer of cell i:

$$\begin{pmatrix} \frac{h^{n*}_i}{N} \\ \frac{h^{n*}_i}{N} v^{n*}_{i,j} \end{pmatrix} - \begin{pmatrix} \frac{h^n_i}{N} \\ \frac{h^n_i}{N} v^n_{i,j} \end{pmatrix} = -\frac{\Delta t^n}{\Delta x} \left(\omega^-_{i,j} \sum_{p:\lambda_p > 0} \left(\mathcal{Z}^p_{i-\frac{1}{2}} - \mathcal{T}^p_{i-\frac{1}{2}} \right) + \frac{1}{N} \sum_{p:\lambda_p > 0} \mathcal{T}^p_{i-\frac{1}{2}} \right.$$
$$\left. \omega^+_{i,j} \sum_{p:\lambda_p < 0} \left(\mathcal{Z}^p_{i+\frac{1}{2}} - \mathcal{T}^p_{i+\frac{1}{2}} \right) + \frac{1}{N} \sum_{p:\lambda_p < 0} \mathcal{T}^p_{i+\frac{1}{2}} \right). \tag{4.32}$$

If a non-flat bottom is considered, the source term contribution is decomposed

together with the flux difference, cf. [5]:

$$\sum_p \mathcal{Z}^p_{i+\frac{1}{2}} = F(U_{i+1}) - F(U_i) - \tilde{S}_{i+\frac{1}{2}} \tag{4.33}$$

$$= \tilde{A}_{i+\frac{1}{2}} \sum_p \mathcal{W}^p_{i+\frac{1}{2}} - \tilde{S}_{i+\frac{1}{2}} = \sum_p \lambda_p \mathcal{W}^p_{i+\frac{1}{2}} - \tilde{S}_{i+\frac{1}{2}}. \tag{4.34}$$

To gain the right flux corrections, we decompose $\tilde{S}_{i+1/2}$ into eigenvectors $\mathcal{S}^p_{i+1/2}$:

$$\begin{pmatrix} 0 \\ -G\tilde{h}_{i+\frac{1}{2}} \end{pmatrix} (b_{i+1} - b_i) = S_{i+\frac{1}{2}} = \sum_p \mathcal{S}^p_{i+\frac{1}{2}}, \tag{4.35}$$

thus we can express the velocity dependent part of the update as follows:

$$\sum_{p:\lambda_p<0} \mathcal{Z}^p_{i+\frac{1}{2}} - \begin{pmatrix} \mathcal{W}^-_{hu} \\ G\tilde{h}_{i+\frac{1}{2}} \mathcal{W}^-_h \end{pmatrix} + \sum_{p:\lambda_p<0} \mathcal{S}^p_{i+\frac{1}{2}} = \begin{pmatrix} 0 \\ \tilde{u}_{i+\frac{1}{2}} \left(-\tilde{u}_{i+\frac{1}{2}} \mathcal{W}^-_h + 2\mathcal{W}^-_{hu} \right) \end{pmatrix}. \tag{4.36}$$

We define, in accordance with the case $b \equiv 0$:

$$\mathcal{T}^p_{i+\frac{1}{2}} := \begin{pmatrix} 0 & 1 \\ G\tilde{h}_{i+\frac{1}{2}} & 0 \end{pmatrix} \mathcal{W}^p_{i+\frac{1}{2}} - \mathcal{S}^p_{i+\frac{1}{2}} \tag{4.37}$$

and can express the weighted update for the system with bottom topography as in (4.32) with the newly defined $\mathcal{Z}^p_{i+1/2}$ and $\mathcal{T}^p_{i+1/2}$.

Note that the additional eigenvector decompositions for the already known eigenvectors and -values of $\tilde{A}_{i+1/2}$ bring little additional numerical cost compared to the monolayer scheme. The only other additional numerical cost comes from calculation of the weights, for which we use a simple and fast interpolation approach.

Remark: Of course negative weights might occur and have to be treated with care. In the case of negative weights the direction in which information travels is reversed, which might lead to instabilities. In our numerical calculations such cases occurred in special test cases, leading to velocities directed against the direction of the mean velocity at this position and thus to a circulating flow. Instabilities did not occur in these cases. Note that the viscous terms add stabilizing effects to the depth-averaged flow.

4.2. Viscous effects

Now, in the second half step the viscous effects are taken into account. Since the viscous term only affects the discharge equation, we set $h_i^{n+1} = h_i^{n*}$.

For the discharge update, we integrate equation (2.26) over the j^{th} layer while neglecting the advection and pressure terms and keeping the layer boundaries constant in time:

$$\partial_t \frac{h}{N} \bar{u}_j(x,t) = \frac{\nu_0}{\varepsilon} \left(\partial_z u(x, \eta_{j-1}(x,t), t) - \partial_z u(x, \eta_j(x,t), t) \right). \tag{4.38}$$

where $\bar{\cdot}_j$ now denotes depth-averaged integration over the j^{th} layer analogous to the depth-averaging over the whole flow in the previous section. At the surface and at the bottom we have boundary conditions prescribing the values for $\partial_z u(x, \eta_j(x,t), t)$. Between two layers we can numerically differentiate to obtain these values. For the layer-wise depth-averaged velocities we assume $\overline{u}_j(x_i, t) \approx v_{i,j}^{n*}$. As a result, the viscous term gives a system with a tri-band matrix (cf. [2]):

$$\begin{pmatrix} a & b & 0 & \dots & 0 \\ b & c & b & \ddots & 0 \\ 0 & b & \ddots & \ddots & \vdots \\ \vdots & \ddots & \ddots & c & b \\ 0 & \dots & 0 & b & d \end{pmatrix} \begin{pmatrix} v_{i,1}^{n+1} \\ \vdots \\ \vdots \\ \vdots \\ v_{i,N}^{n+1} \end{pmatrix} = \frac{h_i^{n*}}{N} \begin{pmatrix} v_{i,1}^{n*} \\ \vdots \\ \vdots \\ \vdots \\ v_{i,N}^{n*} \end{pmatrix} \tag{4.39}$$

with

$$a := \frac{h_i^{n+1}}{N} + \frac{N\nu_0 \Delta t^n}{\varepsilon h_i^{n+1}}, \tag{4.40}$$

$$b := -\frac{N\nu_0 \Delta t^n}{\varepsilon h_i^{n+1}}, \tag{4.41}$$

$$c := \frac{h_i^{n+1}}{N} + \frac{2N\nu_0 \Delta t^n}{\varepsilon h_i^{n+1}}, \tag{4.42}$$

$$d := \frac{h_i^{n+1}}{N} + \frac{N\nu_0 \Delta t^n}{\varepsilon h_i^{n+1}} + \gamma_0 \Delta t^n. \tag{4.43}$$

Solving this system gives the new velocities $v_{i,j}^{n+1}$ and hence the new discharge as a quadrature of the velocity profile using the midpoint rule: $q_i^{n+1} := \frac{h_i^{n+1}}{N} \sum_j v_{i,j}^{n+1}$.

Note that the solution fulfills the following equations for $1 < j < N$:

$$\frac{1}{\Delta t^n} \frac{h_i^{n+1}}{N} \left(v_{i,j}^{n+1} - v_{i,j}^{n*} \right) = \frac{\nu_0}{\varepsilon} \frac{N}{h_i^{n+1}} \left(v_{i,j-1}^{n+1} - 2v_{i,j}^{n+1} + v_{i,j+1}^{n+1} \right) \tag{4.44}$$

$$\Leftrightarrow \frac{1}{\Delta t^n} \left(v_{i,j}^{n+1} - v_{i,j}^{n*} \right) = \frac{\nu_0}{\varepsilon} \left(\frac{N}{h_i^{n+1}} \right)^2 \left(v_{i,j-1}^{n+1} - 2v_{i,j}^{n+1} + v_{i,j+1}^{n+1} \right). \tag{4.45}$$

The latter equation has a discrete backward time-derivative of the velocity at the layer midpoint $(x_i, z_{i,j}^n)$ on the left hand side and a discrete second z-derivative of the same velocity on the right hand side. Hence, it can be viewed as a discrete version of (2.26), where advection and pressure terms have been neglected. Also, the equation 4.44 in the first line is a depth-integrated version over the j^{th} layer of the equation in the second, as $h_i^{n+1} = h_i^{n*}$. Summing up (4.44) for $1 < j < N$ and the corresponding equations for $j = 1$ and $j = N$, we see that the right-hand-side telescopes to yield a numerical approximation of $\mathcal{V}$, while the left-hand-side yields a discrete time-derivative $\left(q_i^{n+1} - q_i^{n*} \right) / \Delta t^n$.

5. The complete scheme

The complete scheme consists of a Finite Volume approximation of the data for the depth averaged equations (2.38), (2.39), i.e., cell-wise constant data U_i^n defining a series of Riemann problems at the cell interfaces. In addition to these data we have velocity vectors v_i^n representing consistent discrete vertical profiles of the horizontal velocities for each cell. The Riemann problems are solved using Roe's solver as described above for a single Riemann problem, yielding the updated data U_i^{n*}. From the numerical fluxes $\Delta t^n/\Delta x \cdot \mathcal{A}_i^{n,\pm}$ at each border of cell i at time t^n we gain update formulas for the velocity vectors to compute the vectors v_i^{n*}. This is done by weighting the numerical fluxes of the total discharge and thus distributing the total flux over the different layers as described above.

Recalling the definition (4.7), for given data U^n, v^n we have the formal definition of the solver:

$$\left.\begin{aligned} \left(U_i^{n*}, v_i^{n*}\right)^T &= \mathcal{SW}_i\left(U^n, v_i^n\right), \\ \left(U_i^{n+1}, v_i^{n+1}\right)^T &= \mathcal{V}_i^n\left(U^{n*}, v_i^{n*}\right). \end{aligned}\right\} \tag{5.1}$$

Collecting the different discretizations detailed in the previous sections, we can now define the operators $\mathcal{SW}_i$ and $\mathcal{V}_i$. For $\mathcal{SW}_i$ we have:

$$\mathcal{SW}_i : \left\{ \begin{array}{rl} U_i^n \mapsto U_i^{n*} & \text{by (3.13)}, \\ (U_i^n, v_i^n) \mapsto v_i^{n*} & \text{by (4.28)}, \end{array} \right\} \text{for } i \in \mathbf{Z}. \tag{5.2}$$

These new velocity vectors v_i^{n*} can then be used to define the right-hand-side of a system of equations modeling the influence of viscosity and bottom friction on the velocity profiles. Implementing this idea, we define the operator $\mathcal{V}_i$ by

$$\mathcal{V}_i : \left\{ \begin{array}{rl} (U_i^{n*}, v_i^{n*}) \mapsto v_i^{n+1} & \text{by (4.39)}, \\ \left(U_i^{n*}, v_i^{n+1}\right) \mapsto U_i^{n+1} & \text{by (4.5)-(4.6)}, \end{array} \right\} \text{for } i \in \mathbf{Z}. \tag{5.3}$$

Now we consider the layer-wise update formulas to compare the numerical scheme with the discrete model for monolayer Shallow Water and with the equations (2.38), (2.39). For the heights we have:

$$\frac{1}{\Delta t^n}\left(\frac{h_i^{n+1}}{N} - \frac{h_i^n}{N}\right) = -\frac{1}{\Delta x}\left(\sum_{p:\lambda_p<0} \frac{1}{N}\left(\mathcal{Z}_{i+\frac{1}{2}}^p\right)_h + \sum_{p:\lambda_p>0} \frac{1}{N}\left(\mathcal{Z}_{i-\frac{1}{2}}^p\right)_h\right). \tag{5.4}$$

Putting together the results (4.32) and (4.44) from the different steps, we get

for the discharge for $1 < j < N$:

$$
\begin{aligned}
&\frac{1}{\Delta t^n}\left(\frac{h_i^{n+1}}{N}v_{i,j}^{n+1} - \frac{h_i^n}{N}v_{i,j}^n\right) \\
&= \frac{1}{\Delta t^n}\left(\frac{h_i^{n+1}}{N}v_{i,j}^{n+1} - \frac{h_i^{n*}}{N}v_{i,j}^{n*} + \frac{h_i^{n*}}{N}v_{i,j}^{n*} - \frac{h_i^n}{N}v_{i,j}^n\right) \\
&= \frac{\nu_0}{\varepsilon}\frac{N}{h_i^{n+1}}\left(v_{i,j-1}^{n+1} - 2v_{i,j}^{n+1} + v_{i,j+1}^{n+1}\right) \\
&\quad - \frac{1}{\Delta x}\left(\sum_{p:\lambda_p<0}\left(\omega_{i,j}^{n+}\left(\mathcal{Z}_{i+\frac{1}{2}}^p - \mathcal{T}_{i+\frac{1}{2}}^p\right)_{hu} + \frac{1}{N}\left(\mathcal{T}_{i+\frac{1}{2}}^p\right)_{hu}\right)\right. \\
&\quad \left. + \sum_{p:\lambda_p>0}\left(\omega_{i,j}^{n-}\left(\mathcal{Z}_{i-\frac{1}{2}}^p - \mathcal{T}_{i-\frac{1}{2}}^p\right)_{hu} + \frac{1}{N}\left(\mathcal{T}_{i-\frac{1}{2}}^p\right)_{hu}\right)\right),
\end{aligned}
\tag{5.5}
$$

where $\omega_{i,j}^{n-}$, $\omega_{i,j}^{n+}$ are defined according to (4.21) and (4.26). The $\mathcal{Z}_{i+1/2,p}$, $\mathcal{T}_{i+1/2,p}$ are defined according to the equations (3.11) and (4.37) as unique eigenvector decompositions of different parts of the flux difference and the source term. Summing up (5.4), (5.5) for $1 < j < N$ and the corresponding equations for $j = 1$, and $j = N$ yields discretizations of (2.38), (2.39), where we can find approximations of each of the different terms in the original PDE. The missing discharge equations for the uppermost and lowest layer only differ in the viscous terms, as here the derivative $\partial_z u$ is given by the boundary conditions (2.29), (2.32) instead of finite differences, cf. (4.40), (4.43).

Note that in the abscence of both bottom and surface friction, any velocity shear which might be present in the initial conditions will reduce due to the viscosity until all velocity profiles are flat. In this case, the second step of the splitting will yield no corrections and the solver reduces to a Finite Volume solver for the Shallow Water equations with topography source term.

5.1. Stability conditions

The ratio between time increment Δt^n and the spatial increment Δx needs to satisfy a CFL-condition:

$$
\max \lambda_{p,i+\frac{1}{2}}^n < cfl\,\frac{\Delta x}{\Delta t^n} \tag{5.6}
$$

with CFL-number $cfl \in (0, 0.5)$ and $\lambda_{p,i+1/2}^n$ the p-th eigenvalue at the interface $i + 1/2$ at time step n. This condition guarantees that the information from the different Riemann-problems at the cell interfaces do not travel beyond the cell midpoints. However, in our case we do not have the actual velocities of the flow in our calculations, as there might be speeds that are faster than eigenvalues calculated using the mean velocities in each cell. These mean velocities are normally not exceeded by far though, which is why we still use this CFL-condition, but with a small CFL-number when we want to prevent interaction

of waves from different cell interfaces. In numerical tests however we did not see problems even with $cfl = 0.8$.

The other important ratio is given by the spatial increment Δx and the number of layers N. As we want to capture smooth transitions properly, the number of layers must not be too big compared to Δx, as then the lowest layers might lose contact with the flow in the next cell. Thus, if the largest jump over a cell interface in the discretized bottom is given by $b_{i+1} - b_i$, which of course depends on Δx for a smooth topography, we impose the condition:

$$\frac{h_i^n}{N} \geq b_{i+1} - b_i \quad \text{for } n \geq 0. \tag{5.7}$$

5.2. Numerical cost

In our numerical calculations for Step 1 we employ the Roe solver for Shallow Water, where we calculated additional decompositions in terms of the eigenvalues, i.e., we solved the equation $Rx = b$ where R is a matrix whose columns are eigenvectors for one additional right hand side b at every cell interface. This is only a small additional contribution to the total cost.

Compared to simple Saint-Venant-type Shallow Water, the main additional contribution to the numerical cost lies in setting up the viscosity matrix and solving the system of equations given by the discretization of the viscous terms. This step is approximately as expensive as the Roe solver for the homogenous Shallow Water equations when we consider 5 to 15 layers for 100 to 200 cells. Of course, as a preparation step we also need an interpolation method to gain the updates for the velocity profiles as described in the previous subsections. The percentage of the computational time needed for the two main numerical routines is shown in table 5.1, where some example calculation were done for different numbers of cells and layers for the test case 4 of the following section, cf. Section 6.5.

The advection routine implements the formulas (5.2) and comprises the calculation of the system matrix entries, the eigenvalues and eigenvectors as well as the update formula for the advective part of the system. As there are analytical formulas for the shallow water system, the calculation of eigenvalues and eigenvectors is quite efficient. The computational time only scales with the number of cells, as the system matrix is of the same size regardless of the number of layers.

The friction routine implements the formulas (5.3) and comprises the calculation of matrix entries of the fricion matrix and the right hand side of (4.39), the solving routine for this linear problem and the correction of the discharge to meet the consistency requirement. For tri-band matrices, the calculation of matrix and vector entries as well as the solving routine have a numerical complexity of $\mathcal{O}(N)$, where N is the number of layers. This linear increase was also reflected in the computational times needed in the example calculations.

Altogether the calculations in the viscous case take approximately twice to thrice as much time as the homogenous case.

number of cells	numerical routine	number of layers		
		5	10	15
100	advection	47.7%	46.9%	45.2%
	friction	36.4%	38,0%	40.1%
150	advection	53.3%	51.6%	49.8%
	friction	37.7%	39.7%	41.8%
200	advection	53.6%	52.1%	49.9%
	friction	38.0%	39.8%	42.4%

Table 5.1: Computational time of the two main numerical routines compared to the total computational time of the solving routine

6. Numerical results

In our numerical tests we used ten layers and set the inverse Froude number to $G = 9.812$ for better comparability with other works.

6.1. Test 1: Convergence test

The first test is a convergence test. As such, the solution to this test is smooth for all times. The initial conditions are set to:

$$h = 2 + 0.1e^{\frac{x^2}{x^2-1}} \qquad \text{for } x \in (-1, 1) \tag{6.1}$$

$$h = 2 \qquad \text{else} \tag{6.2}$$

and the velocities are set to zero:

$$q = hu \equiv 0. \tag{6.3}$$

We set the ratio $\varepsilon = 0.1$ and the viscosity and friction parameters to $\nu_0 = 0.001$ and $\gamma_0 = 0.1$. The initial conditions and the solution at time $t = 0.3$ are plotted in figures 6.3 and 6.4 for 100 Cells and CFL-number $cfl = 0.8$. There is also a comparison with the zero friction and viscosity case, i.e., classical Shallow Water, but the solutions are almost indistinguishable.

At the plotting time, the initial hump on the surface has split up into to humps traveling to the left and the right respectively, both having traveled approximately halfway from the middle to the left of right border of the computational domain. Compared to the homogenous case, there is a slight influence of the friction, as the water height and discharge slightly drag behind and do not reach the peaks of the zero friction calculations, albeit this is barely visible in the plots.

In Table 6.2 we show that the convergence rate goes up to at least 1, where the reference solution is computed on 20480 cells. So the expected convergence rate is met by the scheme.

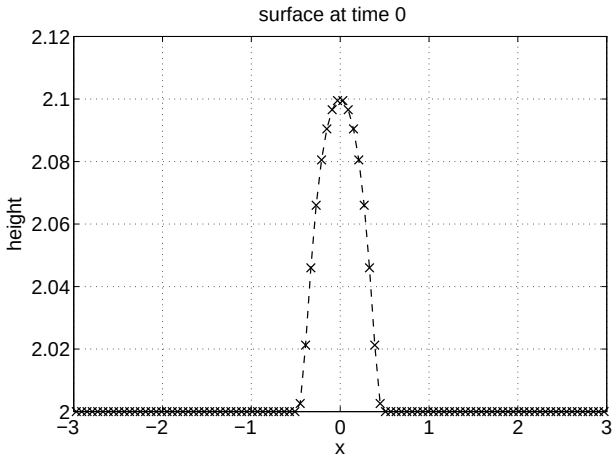

Figure 6.3: Test 1, convergence test, 100 cells, initial condition

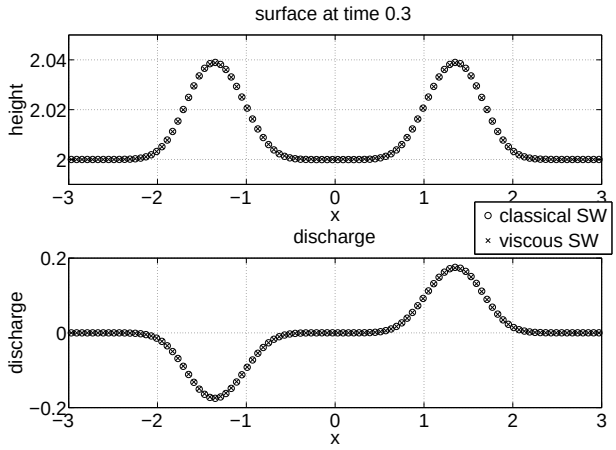

Figure 6.4: Test 1, convergence test, 100 cells, 10 layers, viscous scheme (x) compared with classical Shallow Water scheme (o)

number	h_1		q_1	
of cells	L^1 error	order	L^1 error	order
20	4.7234e-02		2.1034e-01	
40	3.5848e-02	0.40	1.6152e-01	0.38
80	2.2918e-02	0.65	1.0335e-01	0.64
160	1.3231e-02	0.79	5.9608e-02	0.79
320	6.5899e-03	1.01	2.9657e-02	1.01

Table 6.2: Test 1, convergence rates

6.2. Test 2: Subcritical flow

This test was described in [9] as a well balanced test. It will be used now to examine the convergence of our scheme for vanishing viscosity.

The initial conditions desrcibe a subcritical steady state in motion for the non-viscous Saint-Venant equations (2.44)-(2.45). The bottom topography is described by:

$$b = 0.2\, e^{-0.16(x-10)^2} \tag{6.4}$$

for $0 \leq x \leq 25$. The steady state is described by the constant discharge and energy:

$$hu \equiv 4.42 \tag{6.5}$$

$$E = \frac{1}{2}\left(\frac{hu}{h}\right)^2 + G(h+b) \equiv const \tag{6.6}$$

where the constant energy E is defined using the condition $h(0) = 2 - b(0)$. The exact solution to this problem can then be calculated by solving the energy equation for h with

$$\frac{|u|}{\sqrt{Gh}} < 1 \tag{6.7}$$

and the known values of b and the constant hu. The additional condition on another form of froude number in (6.7) gives uniqueness of the solution in this case (cf. equation (2.18) and [18]).

The solution for the homogenous problem is plotted in Figure 6.5. Now, we take the examine convergence by introducing the factor ι and calculate numerical solutions for

$$\varepsilon = 0.1 \tag{6.8}$$

$$\nu_0 = \iota 10^{-2} \tag{6.9}$$

$$\gamma_0 = \iota \tag{6.10}$$

for varying values of ι. As this factor becomes smaller, also the bottom friction and the viscosity decrease and we should see concergence of the profiles and the

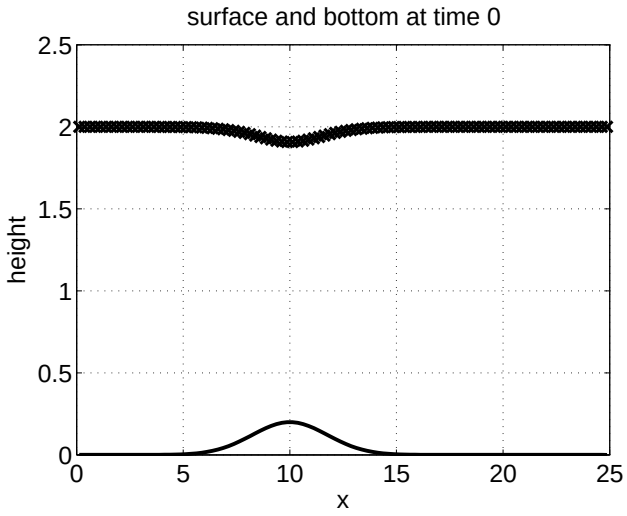

Figure 6.5: Test 2, subcritical flow, 100 cells, 10 layers, steady state for non-viscous system, water heights

soutions to the steady state of the homogenous system as described above. The profiles are plotted in Figure 6.6. As ι becomes smaller, the profiles converge to the mean velocity of the solution to the homogenous system. The smallest values of ι tested lead to profiles which are indistinguishable at plotting resolution.

The deviation for the soultions at $t = 5$ compared to the initial values for these calculations can be found in Table 6.3. The case $\iota = 0$ shows that the scheme is not exactly well balanced, but also that the deviations for small values of ι are governed by the balancing error instead of viscous effects. The convergence is plotted in Figure 6.7.

factor ι	L^1 error h_1	L^1 error q_1
1e-1	1.4900e+000	4.0080e+000
1e-2	2.4160e-001	9.2292e-001
1e-3	2.6105e-002	1.0773e-001
1e-4	2.6947e-003	1.0982e-002
1e-6	1.0182e-004	1.4205e-004
1e-8	9.0081e-005	3.3979e-005
0	9.0042e-005	3.3463e-005

Table 6.3: Test 2, subcritical flow, errors for vanishing viscosity and friction

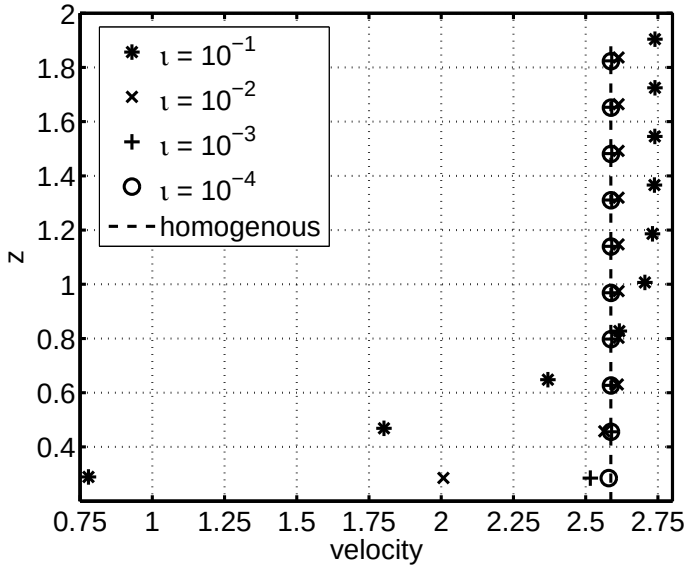

Figure 6.6: Test 2, subcritical flow, velocity profiles for $\iota = 10^{-1}, 10^{-2}, 10^{-3}, 10^{-4}$ and the mean velocity for the homogenous case

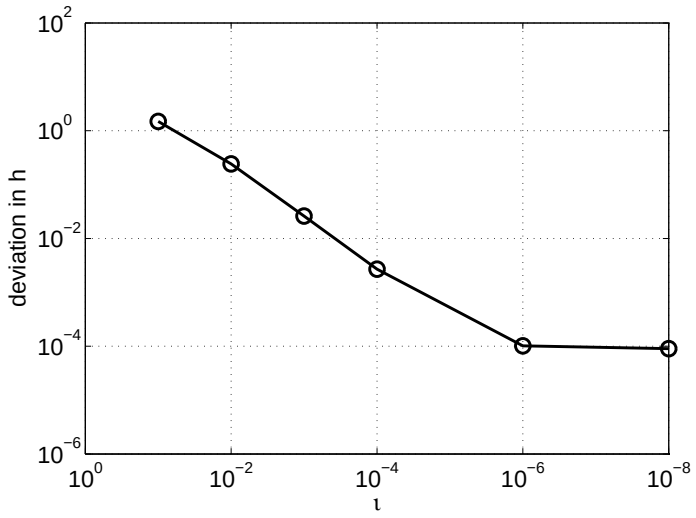

Figure 6.7: Test 2, subcritical flow, deviation in h vs. ι

6.3. Test 3: Dam break

In [15] and [2] a dam-break problem was simulated with two viscous Shallow Water schemes. The initial conditions are:

$$h = 2 \qquad x < 0 \tag{6.11}$$

$$h = 1 \qquad x \geq 0 \tag{6.12}$$

$$hu = 0 \tag{6.13}$$

with $G = 2$ and a flat bottom. Viscosity and friction parameters are set to $\nu_0 = 0.001$, $\gamma_0 = 0.1$, for $\varepsilon = 0.1$, to get the right comparison with the cited references. The plots of the solution at time $t = 14$ calculated with our solver are given in Figure 6.8 and Figure 6.9. As a reference also the solution for a classical Shallow Water solver without friction and viscosity, i.e. a solver for the homogenous Shallow Water equations, is given.

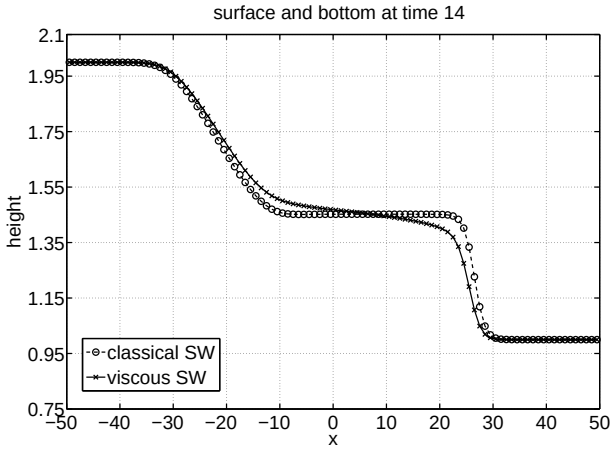

Figure 6.8: Test 3, dam-break problem, 100 cells, 10 layers, time $t = 14$, water heights, classical non-viscous scheme and viscous scheme

Compared to the classical Shallow Water solver, we get an inclined surface between the rarefaction and the shock, as we can also observe in the above references. In the discharge plot we can see the slowing effect of the bottom friction.

The velocities at the layer midpoints are given in Figure 6.10. Compared to [2] the positions of the layer midpoints vary, as we calculate the layer heights as $1/N$ of the total height, whereas in the reference the heights are calculated by transport relations. However, we see similar minimal and maximal values for the velocities.

In Figure 6.11 we see the velocity profile in detail at the position $x = 7.5$. For better comparison, we plotted the profile with the axis found in [2]. Comparing the two profiles, we see a deviation at the bottom, but reach the same velocities close to the surface.

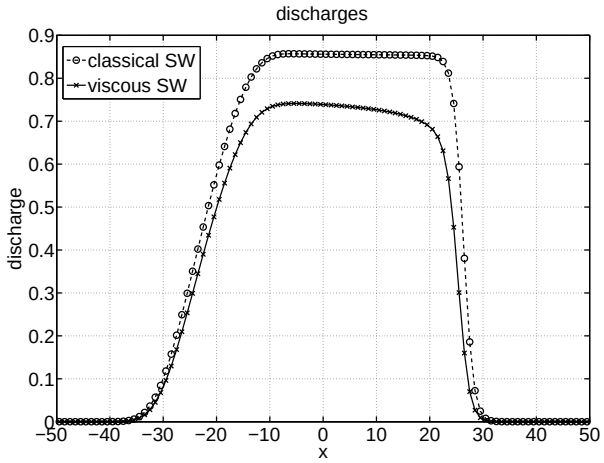

Figure 6.9: Test 3, dam-break problem, 100 cells, 10 layers, time $t = 14$, discharges, classical non-viscous scheme and viscous scheme

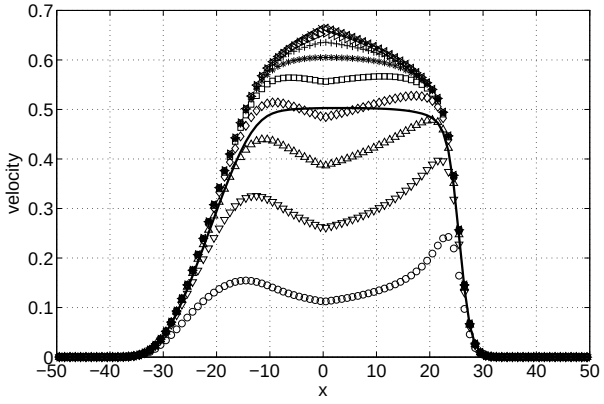

Figure 6.10: Test 3, dam-break problem, 100 cells, 10 layers, velocities at the layer midpoints z_j, crosses marks highest, circles lowest layer, solid line: mean velocity, see also Fig. 6.11 for height-ordering of the velocities

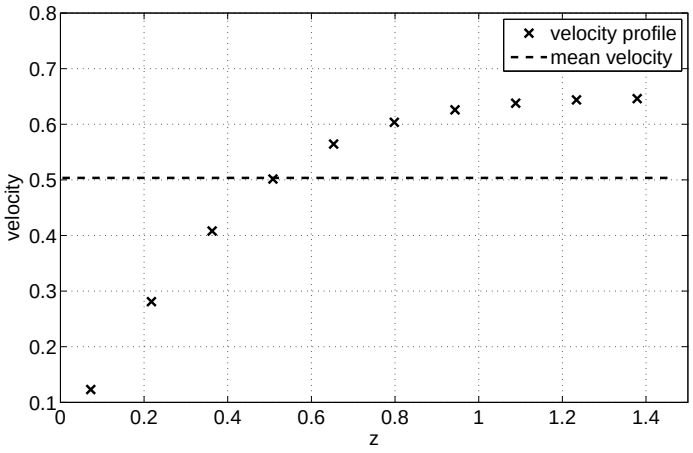

Figure 6.11: Test 3, dam-break problem, 10 layers, velocity profile at $x = 7.5$

Our results are similar to the results of [15] and [2], which in turn are similar to calculation for the full Navier-Stokes equations. Compared to [15] we do not fix the form of the profile as a quadratic polynomial but let the profile develop according to discrete viscosity terms. Compared to [2], we save the time for the costly solving of a $2N \times 2N$ system in the first half step.

6.4. Test 4: Flow down a slope

In this test case we examine a certain kind of balance situation. The flow is running down a slope, with the acceleration due to gravity and the slowing effect of the bottom friction reaching a balance after some time. So the flow reaches a stead state with constant height h and constant discharge $hu > 0$ even though the bottom is not constant. This steady state is achieved by assuming certain boundary conditions at the left border.

The initial conditions are:

$$h = 0.1 \tag{6.14}$$

$$hu = \frac{G}{3}, \tag{6.15}$$

with $G = 10$, $\nu_0 = 10^{-5}$, $\gamma_0 = 0.020689552$, $\varepsilon = 0.1$ and the bottom topography is given by:

$$b(x) = 1 - 0.1x. \tag{6.16}$$

The physical parameters are chosen to resemble the parameters used in a thesis work by K. Kloss [16]. In that thesis Test 4 was performed for a Shallow Water scheme with a analytically gained quadratic profile u_{poly} for the velocity using a no-slip friction condition at the bottom, $\partial_z u = 0$ at the surface and $\int_b^\eta u_{poly}(z)\,\mathrm{d}z = u$. The resulting profile reads:

$$u_{poly}(z) = -\frac{3}{2}\frac{u}{h^2}(z - z_0)^2 + \frac{3}{2}\frac{u}{h}(z - z_0) + \frac{9}{8}u, \tag{6.17}$$

where $z_0 = 0.5(\eta - b)$.

The values given in (6.14) are already the values when steady state is reached. However, as the simulation is started with a constant velocity profile, it takes some iterations to actually reach the steady state with the correct profile in every cell.

The boundary condition at the left border is realized using a ghost cell, in which we fix the height and discharge to the values given above in (6.14), $b(x)$ is simply evaluated at the ghost cell midpoint. The velocity profile for ten layers is calculated from the balance condition between friction and acceleration due to the bottom topography, see Figure 6.12.

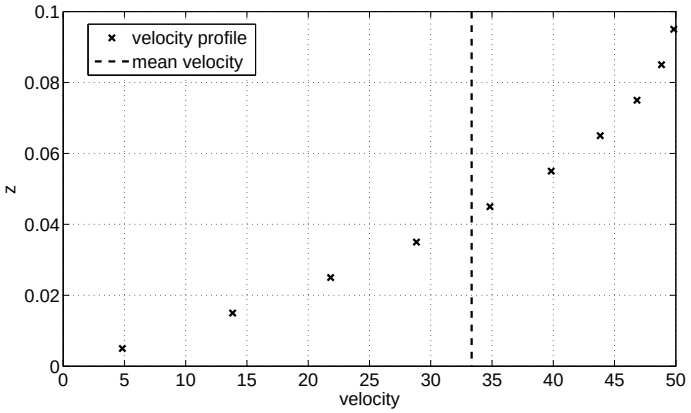

Figure 6.12: Test 4, flow down a slope, 10 layers, velocity profile prescribed at left boundary, dashed line: mean velocity, z giving height above bottom b in this plot

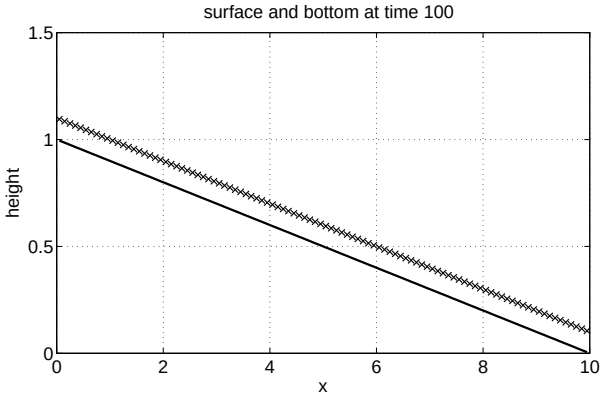

Figure 6.13: Test 4, flow down a slope, 100 cells, 10 layers, steady state reached, bottom friction and gravitational acceleration in balance

Thus, the predicted steady state (see figs 6.13, 6.12) is reached with our

scheme. Compared to results with the quadratic polynomial described above as prescribed profile for the velocities, we notice deviations in the order of 10^{-13} when comparing the mean velocities of the different layers.

6.5. Test 5: Transcritical flow

In this test we simulate a transcritical flow over hump. This test was performed in [18] as a test for moving equilibria in a non-viscous Shallow Water flow.

The initial data is set to:

$$h = 0.66 \tag{6.18}$$

$$q = 1.53 \tag{6.19}$$

and the bottom topography is set to:

$$b = \begin{cases} 0.2 - 0.05(x-10)^2 & \text{if } 8 \leq x \leq 12 \\ 0 & \text{otherwise} \end{cases} . \tag{6.20}$$

At the left border we impose $hu = 1.53$ as a boundary condition. The friction and viscosity parameters are set to $\gamma_0 = 10^{-4}$ and $\nu_0 = 10^{-5}$ for $\varepsilon = 0.1$.

The solution at time $t = 10$ for 100 grid cells is shown in Figure 6.14 with a detailed look on the velocities computed for 200 grid cells at the same time in Figure 6.15. The vertical components of the velocities are gained by a numerical integration, based on the kinematic and no-penetration boundary conditions as well as the vanishing divergence for this incompressible flow.

In Figure 6.15 the flow actually shows a recirculation after the hump, where the upper layers flow slowly against the direction of the mean velocity and the direction of the lower layers. Also, in the shock we can see where the recirculation starts, as the upper layers are accelerated downward and upstream due to the pressure gradient and kinematic boundary condition. The comparison of the total height and discharge however show only a small deviation, where the viscous scheme is dragging slightly behind due to the bottom friction. So the scheme offers a more detailed view on the non-trivial velocity profiles while not changing the solution too much.

The steady state is reached at about time $t = 30$ and is shown in figure 6.16. It shows little deviation from the non-viscous scheme and is indistinguishable at plotting precision, hence we omit the non-viscous solution in this figure.

7. Conclusion

In this paper we described the derivation of a Shallow Water model with viscous terms and a Navier friction condition at the bottom. For this model a suitable Roe-type Finite Volume scheme with an additional treatment of the viscosity and friction terms has been defined.

Describing the vertical profile of the horizontal velocities in terms of discrete point values, we were able to define an update formula of this profile respecting

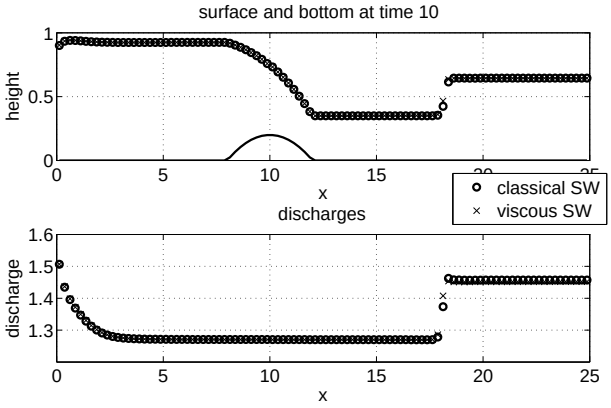

Figure 6.14: Test 5, transcritical flow over a hump, 100 cells, 1- layers, $t = 10$

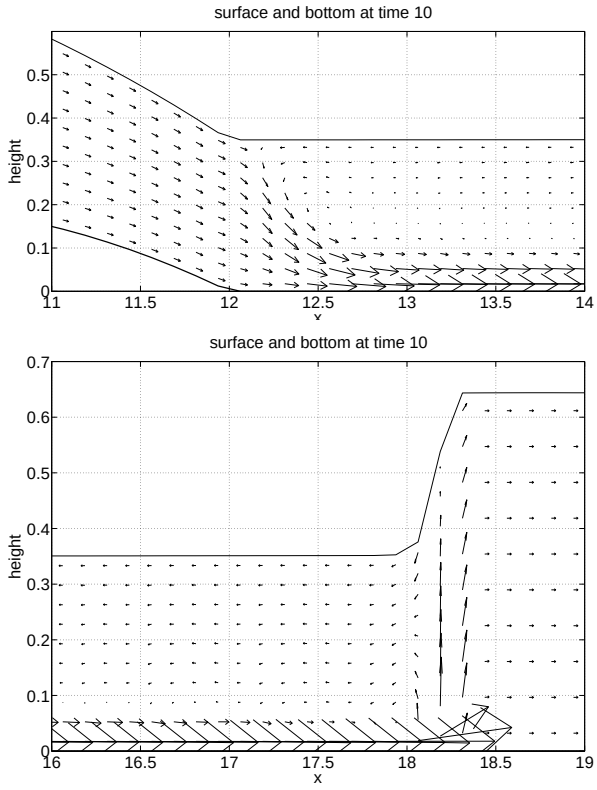

Figure 6.15: Test 5, transcritical flow over a hump, 200 cells, 10 layers, detailed view on velocities at the downstream side of the hump and in the downstream moving shock

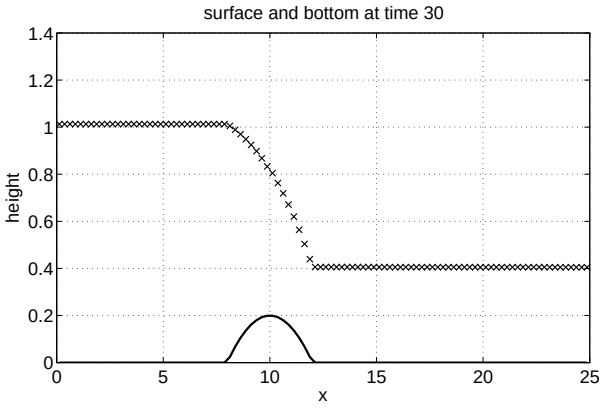

Figure 6.16: Test 5, transcritical flow over a hump, 100 cells, 10 layers, steady state

the update formula of the total mass and total discharge equations. This was achieved by a splitting of velocity and non-velocity related terms in the discharge equation and a weighting procedure with weights defined in terms of local velocities at the cell interfaces. The splitting allows for recirculation at shocks, as the inflow regions at a cell interface may be restricted to a certain region in the depth-direction, so the acceleration due to the local pressure gradient is only countered by the relatively small viscous effects. In a second update step, the viscous effects were treated by an implicit time discretization like described in [2] yielding, after a numeric depth integration, a corrected total discharge.

The scheme successfully computed several numerical tests with the expected results or results close to other schemes for Shallow Water flows respecting viscosity and bottom friction. The additional numerical costs are moderate and mostly due to the implicit solver for the depth-discretization of the viscous terms.

Test 3 shows that our results compare well against other viscous shallow water solvers. The advantages of our solver are that we can include non-vanishing surface friction more easily than the solver of [15], while improving on the computational effort of the solver of [2].

In [14], we describe how to enhance the viscosity treatment to the density-layered Shallow Water flows. The goal was to get a finer resolution of the different physical effects acting on these kinds of flows as well as at least partly cure the instabilities occurring due to large shear velocities, which should be counteracted by the viscous effects. In this work, the flexibility of discrete velocity profiles compared to pre-defined (parabolic) profiles was crucial as the density layers experience non-vanishing shear stress at both the lower and the upper interface.

8. Acknowledgments

The author wishes to thank Manuel Castro, Carlos Parés, Sebastian Noelle and Gabriella Puppo for inspiring discussions leading to the development of the basic ideas of this work. Financial support from the Deutsche Forschungsgemeinschaft (German Research Foundation) through grant GSC 111 is gratefully acknowledged.

[1] R. Abgrall, S. Karni, Two-layer shallow water system: a relaxation approach, SIAM J. Sci. Comput. 31 (2009) 1603–1627.

[2] E. Audusse, A multilayer Saint-Venant model: derivation and numerical validation, Discrete Contin. Dyn. Syst. Ser. B 5 (2005) 189–214.

[3] E. Audusse, M.O. Bristeau, Finite-volume solvers for a multilayer Saint-Venant system, Int. J. Appl. Math. Comput. Sci. 17 (2007) 311–319.

[4] E. Audusse, M.O. Bristeau, M. Pelanti, J. Sainte-Marie, Approximation of the hydrostatic Navier-Stokes system for density stratified flows by a multilayer model: kinetic interpretation and numerical solution, J. Comput. Phys. 230 (2011) 3453–3478.

[5] D.S. Bale, R.J. LeVeque, S. Mitran, J.A. Rossmanith, A wave propagation method for conservation laws and balance laws with spatially varying flux functions, SIAM J. Sci. Comput. 24 (2003) 955–978.

[6] F. Bouchut, Nonlinear stability of finite volume methods for hyperbolic conservation laws and well-balanced schemes for sources, Frontiers in Mathematics, Birkhäuser Verlag, Basel, 2004.

[7] F. Bouchut, T. Morales, An entropy satisfying scheme for two-layer shallow water equations with uncoupled treatment., M2AN Math. Model. Numer. Anal. 42 (2008) 683–698.

[8] M. Castro, J. Frings, S. Noelle, C. Pares, G. Puppo, On the hyperbolicity of two- and three-layer shallow water equations, in: Hyperbolic Problems. Theory, Numerics and Applications (Editors: Tatsien Li; Song Jiang), volume 1, Higher Education Press, Beijing, 2012, pp. 337–345.

[9] M. Castro, J.M. Gallardo, C. Parés, High order finite volume schemes based on reconstruction of states for solving hyperbolic systems with nonconservative products. Applications to shallow-water systems, Math. Comp. 75 (2006) 1103–1134 (electronic).

[10] M. Castro, J. Macías, C. Parés, A Q-scheme for a class of systems of coupled conservation laws with source term. Application to a two-layer 1-D shallow water system, M2AN 35 (2001) 107–127.

[11] M.J. Castro, J.A. García-Rodríguez, J.M. González-Vida, J. Macías, C. Parés, M.E. Vázquez-Cendón, Numerical simulation of two-layer shallow water flows through channels with irregular geometry, J. Comput. Phys. 195 (2004) 202–235.

[12] M.J. Castro, J. Macías, C. Parés, J.A. García-Rodríguez, E. Vázquez-Cendón, A two-layer finite volume model for flows through channels with irregular geometry: computation of maximal exchange solutions. Application to the Strait of Gibraltar, Commun. Nonlinear Sci. Numer. Simul. 9 (2004) 241–249.

[13] M. Castro-Díaz, E. Fernández-Nieto, J. González-Vida, C. Parés-Madronal, Numerical treatment of the loss of hyperbolicity of the two-layer shallow-water system, Journal of Scientific Computing 48 (2011) 16–40. 10.1007/s10915-010-9427-5.

[14] J.T. Frings, An Adaptive Multilayer Model for Density-layered Shallow Water Flows, Ph.D. thesis, RWTH Aachen, 2012.

[15] J.F. Gerbeau, B. Perthame, Derivation of viscous Saint-Venant system for laminar shallow water; numerical validation, Discrete Contin. Dyn. Syst. Ser. B 1 (2001) 89–102.

[16] K. Kloss, Flachwassergleichungen mit quadratischem Geschwindigkeitsprofil: Modellierung, Numerik und korrekte Bilanzierung von Gleichgewichten, Diplom thesis, RWTH Aachen University, 2010.

[17] R.J. LeVeque, Numerical methods for conservation laws, Lectures in Mathematics ETH Zürich, Birkhäuser Verlag, Basel, second edition, 1992.

[18] S. Noelle, Y. Xing, C.W. Shu, High order well-balanced finite volume WENO schemes for shallow water equation with moving water, J. Comput. Phys. 226 (2007) 29–58.

[19] P.L. Roe, Approximate Riemann solvers, parameter vectors, and difference schemes, J. Comput. Phys. 43 (1981) 357–372.

[20] C.B. Vreugdenhil, Numerical methods for shallow-water flow, Water science and technology library, Kluwer Academic Publishers, 1994.